Use of microfibrillated cellulose and dendritic copper for the elaboration of conductive films from water- and ethanol-based dispersions

Olivier Pras · Davide Beneventi · Didier Chaussy · Paul Piette · Sandra Tapin-Lingua

Abstract In this study, microfibrillated cellulose (MFC) and dendritic copper were used as binder and conductive phase for the elaboration of self-standing conductive films and coatings. A filtration technique was used to prepare MFC/Cu films from particle dispersions in water and ethanol. In aqueous slurries copper oxidized and an additional corona treatment or the use of zinc particles as sacrificial anode were necessary to obtain films with conductivities ranging from 70 to 2500 S m^{-1}, respectively. In ethanol-based MFC/Cu slurries, copper was subjected to limited oxidation. However, the low packing density of conductive particles (below the percolation threshold) led to resistive films which, after densification by calendering, displayed extremely high conductivities, up to 70000 S m^{-1}. Aqueous MFC/Cu slurries were successfully used for the deposition of conductive coatings on copy paper by Mayer rod coating and screen printing, which were subsequently treated by corona discharge and calendering. The obtained coatings displayed intermediate conductivity (i.e. 95 and 570 S m^{-1} for rod coating and screen printing, respectively), which can be further increased using zinc particles or ethanol-based formulations.

O. Pras · D. Beneventi (✉) · D. Chaussy
Grenoble Institute of Technology, UMR 5518 CNRS-Grenoble-INP, Domaine Universitaire, 461 rue de la Papeterie, BP 65, 38402 St. Martin d'Hères, France
e-mail: davide.beneventi@pagora.grenoble-inp.fr

O. Pras · P. Piette
Centre Technique du Papier (CTP), DU, BP 251, 38044 Grenoble Cedex 9, France

S. Tapin-Lingua
FCBA-Pôle Nouveaux Matériaux, Domaine Universitaire, CS 90251, 38044 Grenoble Cedex 9, France

Introduction

Over the past years, the development of new printed electronic devices suitable for low-cost applications [1, 2], such as RFID tags [3, 4], rollup displays [5] and associated energy storage systems [6], induced an ever increasing demand for highly conductive coatings and films to be used both as conductive paths or electrodes for devices wiring and assembly [7].

Paper-like electrodes with improved flexibility have been obtained with carbon nanotube (CNT)–polymer composites [8, 9] and by CNT ink deposition onto flexible polymer substrates [10], paper [11, 12] and textiles [13]. Paper sheets made of graphene and graphene oxide have also been fabricated with resulting conductivity up to 1.2×10^4 S m^{-1} after heat treatment at 220 °C [14]. Owing to their high chemical stability and their availability in various forms [15], graphitic fibres and particles represent the material of choice for the production of conductive coatings and films. Nevertheless, the highest conductivity attainable by these coatings, which roughly corresponds to a fraction of the intrinsic conductivity of bulk graphite (i.e. 2.2×10^6 S m^{-1} [16]), can represent a limitation when highly conductive thin films are required. Thereafter, metallic conductors are more adequate. The main advantage of using metal particles as conductors is the high film conductivity that can be attained after annealing, ca. 10^7 S m^{-1} [17–19]. The type of metal used as conducting material in an electronic application depends on several factors, including the requirements on the conductivity, work function, oxidation stability (in air), fabrication

techniques and cost. While, most of the researches focused on precious metals, such as gold and silver nanoparticle systems [19–21], conductive ink containing copper nanoparticles have been recently developed as low-cost alternative [17, 18, 22].

However, owing to a high inter-particle contact area in nanoparticle systems, organic dispersants carbonization and metal sintering are generally required to attain high film conductivity. In most of cases, in the absence of severe thermal treatment (>250 °C) copper nanoparticle films display a resistive behaviour and conductivity does not attain 10^{-1} S m^{-1} [17]. Thereafter, micrometre-sized copper powders with dendritic/fibrous geometry [23, 24] and high axial ratio [25] remain a material of choice for the elaboration of polymer-based conductive films.

Despite the extensive use of copper for the elaboration synthetic polymer/Cu bulk composites [24, 26, 27] the use of wood polymers as non-conductive binder has been disregarded, and only one work [28] reports the use of dendritic copper powders and lignocellulose microparticles for the elaboration of conducting porous composites with limited mechanical properties. Among lignocellulosic materials, microfibrillated cellulose (MFC) appears as the material of election to be used as binder for conductive fillers. MFC, first obtained by Herrick and Turbak [29, 30], is constituted by long and flexible cellulose nanofibres with ca. 1–100 nm diameter, 200–1000 nm length [31] and consisting of alternating crystals and amorphous strings. When dispersed in water MFC has a web like structure [32] and, owing to its high mechanical properties [33], it has been used as a rheology modifier [34], in foods, paints, cosmetics, pharmaceutical products, and as a reinforcing agent in polymer nanocomposites [35]. Recently, MFC/polypyrrole [36] and MFC/graphite [37] composites with improved electrical conductivity and mechanical properties have been obtained by film casting from aqueous slurries. Moreover, hydrocolloid suspensions and quick filtration techniques have been used for the elaboration of MFC/inorganic hybrid nanocomposites coupling excellent toughness to gas barrier/fire retardancy [38, 39] or electrochemical properties [40, 41].

The aim of this study was to use MFC, dendritic copper and a quick filtration method for the elaboration of tough and highly conducting hybrid composites in the form of self-standing films and coatings.

Materials and Methods

Dendritic copper micro-particles with nominal average size of 3 μm and spherical zinc particles with diameter smaller than 10 μm were used as conductive phase and for copper cathodic protection, respectively. Both metal particles were supplied by Sigma-Aldrich and used as received. SEM images in Fig. 1 show that despite their nominal size, dendritic copper and zinc particles are present in form of large clusters and spherical particles with size close to 40 and 2–10 μm, respectively.

MFC was produced with a sulphite-bleached spruce pulp (supplied by Domsjö). The industrial pulp was disintegrated in water at 5 % consistency for 15 min. A prerefining stage was then carried out using a 12″ single-disc pilot refiner system on 5 kg of o.d. pulp. The objective of this first refining stage was to obtain a slightly refined pulp with a drainage index close to 25 SR. An enzymatic treatment was then applied on the prerefined pulp with a commercial cellulase, Novozym 476 (Novozymes, Denmark), at a dosage of about 1 mL kg$^{-1}_{pulp}$ and an incubation time of 2 h at 50 °C.

Subsequently, a second refining stage was performed on the enzymatically pre-treated pulp. The objective of this intensive refining was to cut fibres, to obtain a fibre length between 300 and 400 μm and to enhance microfibrillation. This second refining stage was performed using the same 12″ single-disc refiner used in the pre-refining step.

The final pulp was then processed at a constant volumic flow of 350 mL min^{-1} in a microfluidizer (Microfluidics M-110EH model) equipped with 3 Z-like chambers with internal diameter of 400, 200 and 100 μm, respectively. The pulp was passed one, three and five times in the 400, 200 and 100 μm chambers, respectively.

SEM analysis (Fig. 1) allowed to estimate the average length and diameter of MFC to ca. 1–5 μm and 50 nm and highlighted the presence of MFC with 500 nm diameter, thus reflecting incomplete microfibrillation.

The pristine, 2 % concentration, MFC–water gel was diluted in water to a MFC concentration of 1 % in weight. After 2 min stirring, copper particles were added to the MFC dispersion in order to obtain a metal weight fraction (given with respect to the Cu and MFC cumulative mass) ranging between 80 and 97 %.

Some samples were prepared adding zinc particles to the MFC/Cu dispersions in order to obtain a Zn weight fraction (with respect to the Cu and Zn cumulative mass) ranging from 0 to 15 %. The cumulative weight fraction of Cu and Zn particles was kept constant to 97 % thorough all experiments.

Before use, dispersions were diluted at a dry solid concentration of 1 % and mixed with a magnetic stirrer during 10 min.

In order to evaluate the impact of the dispersing medium on the film properties, MFC/Cu dispersions were also prepared using ethanol. The pristine MFC–water gel was mixed with ethanol with a 1:1 weight ratio and centrifuged during 15 min at 4000 rpm. The supernatant (mainly composed by a MFC–ethanol dispersion) was removed and
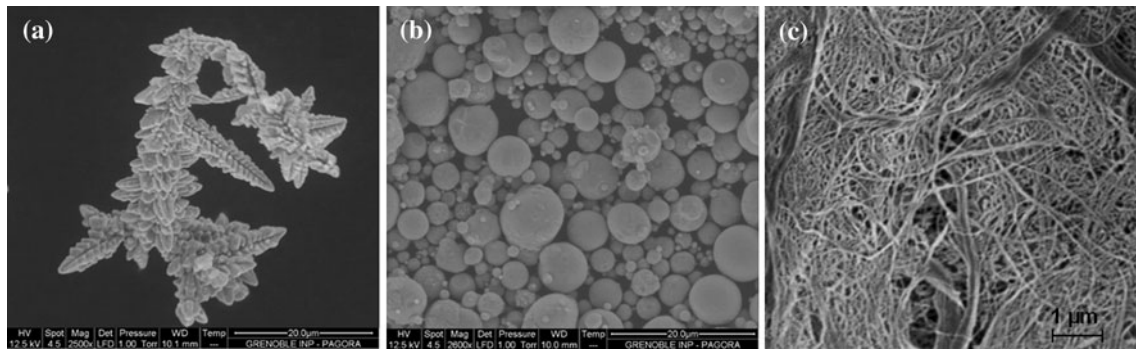
Fig. 1 Materials used for the elaboration of conductive films. **a** Dendritic copper particles, **b** spherical zinc particles and **c** MFC

submitted to the same process five times. Ethanol was then added to the obtained dispersion to adjust MFC concentration to 1 %. MFC/Cu dispersions were then prepared following the same procedure used for aqueous dispersions.

Conductive paper-like films were prepared by filtrating 17 g of the 1 % MFC–metal particles dispersion in a Buchner funnel wear with a 1 μm threshold Teflon filter. The obtained mat (42 mm diameter) was placed between a carrier board (200 g m^{-2}) and a paper cover-sheet (65 g m^{-2}). A couch roll (120 mm diameter, 250 mm length and 3.0 kg mass) was rolled back and forth over the sheet along two perpendicular directions. The obtained pileup was then dried under vacuum at 90 °C during 10 min (Fig. 2).

In order to improve conductivity, MFC/Cu films were also treated with a corona surface treatment (SG2 Calvatron generator, tension of 20 kV at 20 kHz, current intensity of 245 mA and film treatment time of 2.5 s) and a soft calender [42] (laboratory soft-calender RK22-H Ramisch & Co) without heating the stainless steel reel and at 90 °C. The width of the calender nip was measured under static conditions using copy paper sandwiched between paper sheets in order to obtain the same thickness of MFC/Cu films. The average pressure in the load area was then calculated as

$$P = \frac{F}{L \cdot W_{nip}} \tag{1}$$

where F is the force applied on the calender reels, L is the nip length and W_{nip} is the experimentally determined nip width.

Conductive coatings were also deposed on commercial copy paper using high concentration MFC/Cu dispersions by both Mayer rod coating (Elcometer 4340 with 5 cm s^{-1} coating speed and 950 μm gap between the rod and the support) and screen printing (Horizon 03I, DEK).

The morphology of films and coatings was imaged by SEM and their thickness was measured with an Adamel Lhomargy MI20 caliper. The apparent density of the films was evaluated using the measured volume and weight of the samples, whereas nominal Cu and cellulose densities were used to calculate the film porosity (ϕ_{Air}) and Cu and MFC volume fractions (ϕ_{Cu}, ϕ_{MFC}):

$$\phi_{Air} \cong W_{Cu}\left(1 - \frac{\rho_{App}}{\rho_{Cu}}\right) + W_{MFC}\left(1 - \frac{\rho_{App}}{\rho_{Cell}}\right) \tag{2}$$

$$\phi_{Cu} = W_{Cu}\frac{\rho_{App}}{\rho_{Cu}} \tag{3}$$

$$\phi_{MFC} = W_{MFC}\frac{\rho_{App}}{\rho_{Cell}} \tag{4}$$

Fig. 2 Scheme of the film fabrication process

Heating at 90°C during 10 min

Aspiration
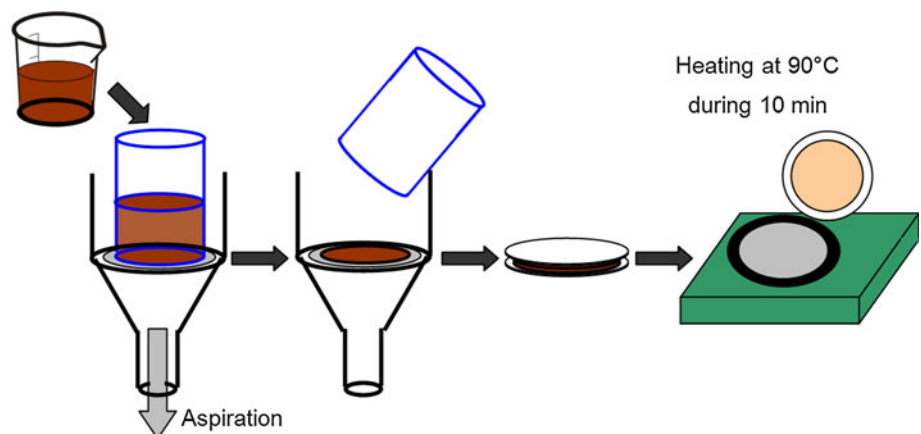
where ρ_{App} is the film apparent density (volumic weight), ρ_{Cu} and ρ_{Cell} are copper and cellulose densities and W_{Cu} and W_{MFC} are copper and MFC weight fractions in the film.
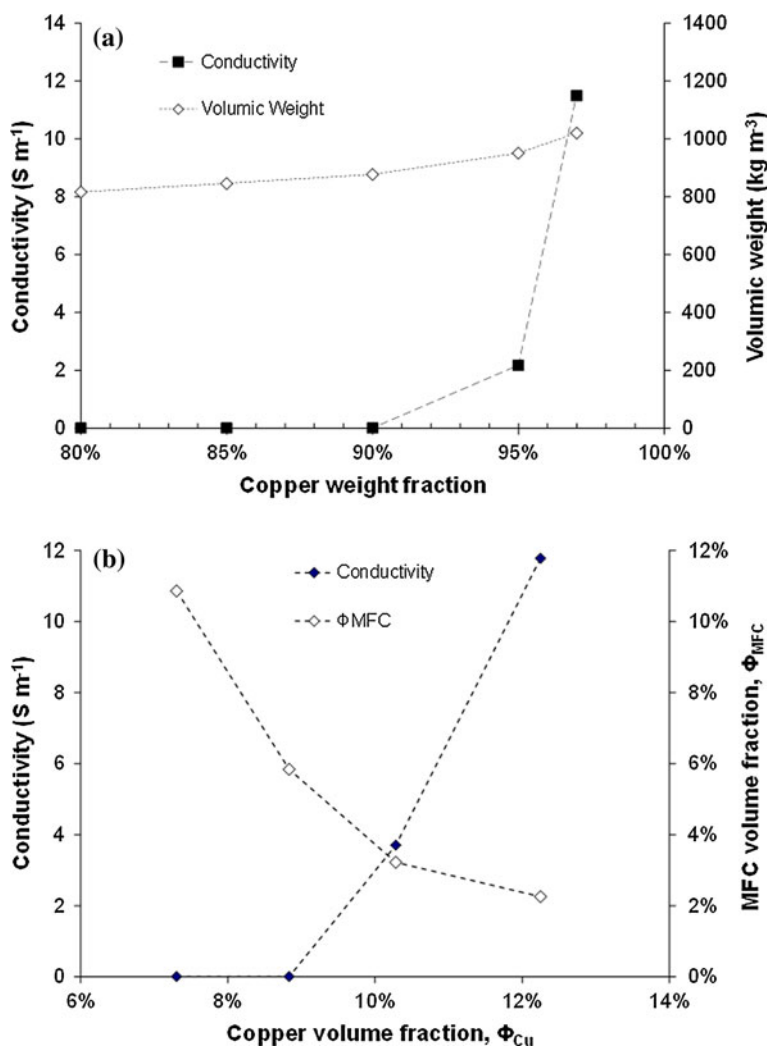
The conductivity of MFC/Cu films and coatings was determined using a 4-probes technique (Jandel Universal probe coupled with a RM3 current generator). The bulk conductivity, σ, was calculated as

$$\sigma = \frac{I}{V}\frac{K}{e} \tag{5}$$

where I is the applied current, V is the measured voltage, e is the sample thickness and K is a geometric parameter (0.22 for the tested geometry).

Traction tests were performed at room temperature (25 °C, no relative humidity control) with a velocity of 0.001 mm s^{-1} using a RSA 3 device (TA Instrument). Samples had 5.5 mm × 20 mm rectangular shape and the gap between the DMA clamps was equal to 10 mm (5 supplementary mm were used at each side to fix the sample).

Results and discussion

Figure 3a shows the conductivity and the apparent density of MFC/Cu conductive films containing increasing weight fractions of Cu.

For a Cu weight fraction lower than 90 %, no conduction is detected. Above this value, which was considered as the critical weight fraction for the formation of a percolation path among conductive particles [43], electron conductivity progressively increases up to 11.5 S m^{-1} for a Cu content of 97 %. The extremely high weight fraction of Cu needed to attain the percolation threshold was due to the low density of MFC/Cu films which ranges between 815 and 1020 kg m^{-3}, is far below cellulose and Cu densities (i.e. 1500 and 8960 kg m^{-3}, respectively). MFC/Cu films porosity ranged between 80 and 90 % and, since MFC films (in the absence of Cu) and tapped dry Cu particles had 50 and 86 % porosity, respectively, it was assumed that MFC/Cu film formation was dominated by the packing of stiff Cu particles.

Fig. 3 Influence of Cu weight **a** and volume **b** fraction on the electric conductivity of MFC/Cu films

The plot of film conductivity as a function of the copper volume fraction, Fig. 3b, shows that the volumic percolation threshold of dendritic Cu particles used in this study is ca. 9.5 % and close to that of particles with similar size and shape [23, 28].

Even in the presence of an extremely high Cu content, MFC/Cu films displayed low conductivity 11.5 S m^{-1} which was ascribed to high film porosity and to the formation of a low conductivity copper oxide layer (ca. 10^{-2} S m^{-1} against 5.9×10^7 S m^{-1} for bulk Cu) on Cu particles in contact with water. The corona discharge was therefore used as surface etching treatment [44] to remove the oxide layer and improve film conductivity.

Figure 4 shows that the corona treatment led to an increase of the electric conductivity of the films. Indeed, when increasing the exposure time to the corona discharge the conductivity increases from 10 to 75 S m^{-1}. However, above 12.5 s exposure (corresponding to 5 treatments) conductivity levels off. Despite a sevenfold increase in conductivity, the etching of the MFC/Cu film by the corona discharge was not sufficient to completely remove the oxide layer from the surface of Cu particles, moreover, after one week, conductivity dropped down to 10 S m^{-1} indicating oxide reformation.

With the aim of preventing copper particles oxidation during the dispersion and film formation stages, and

Fig. 4 Influence of the corona treatment on the conductivity of the films. Cu weight fraction of 97 %. Each treatment corresponds to 2.5 s exposure of the film to a 20 kV corona discharge
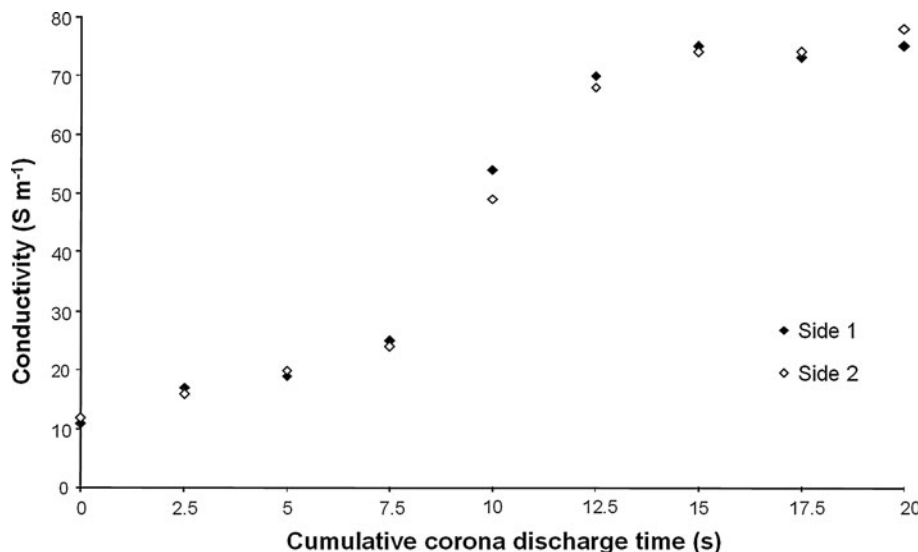
Fig. 5 MFC/Cu/Zn films, influence of the Zn weight fraction (given with respect to the total metal mass) on the conductivity and apparent density of films with a constant metal weight fraction of 97 %. The *inset* represents a SEM micrograph of the surface of a film containing 97 % in mass of metal (95 % Cu and 5 % Zn) and 3 % MFC
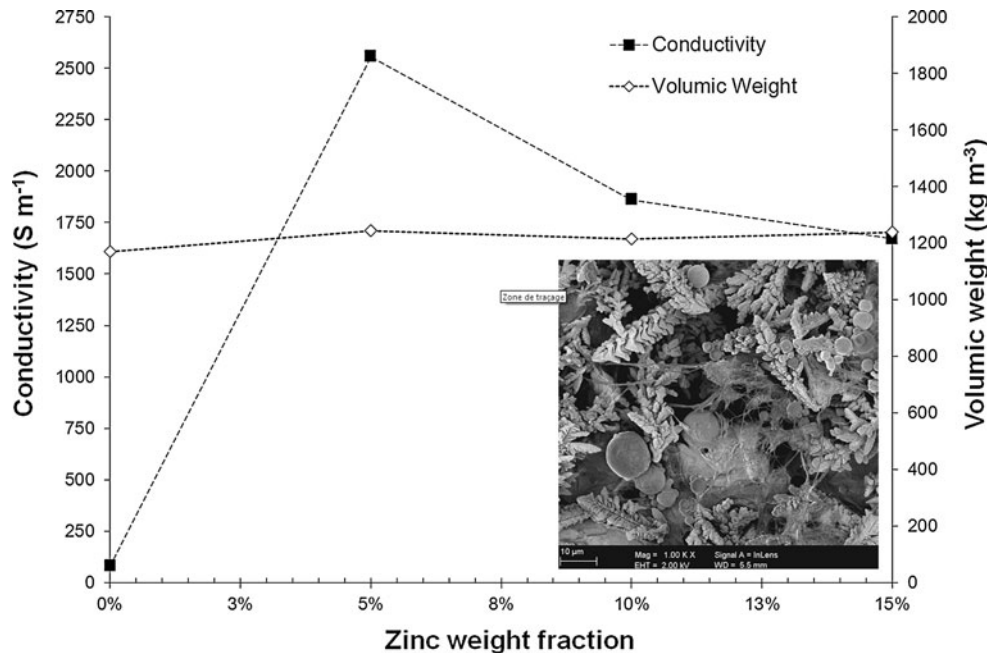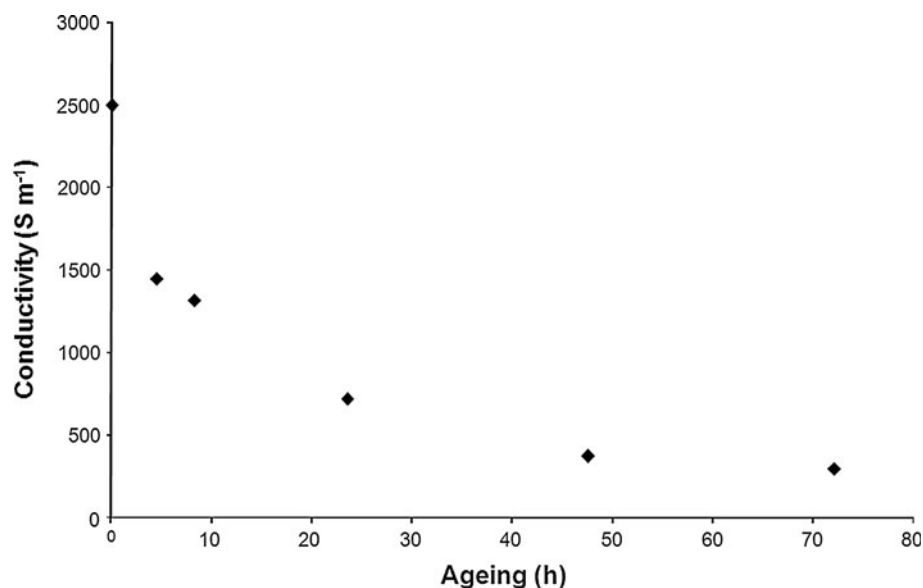
Fig. 6 Impact of film ageing at room conditions on MFC/Cu/Zn films conductivity. Total metal weight fraction 97 %, Zn weight fraction 5 % (with respect to the total metal mass)

according to the standard electrode potential for Cu^{2+}/Cu (0.34 V) and Zn^{2+}/Zn (−0.76 V) [45], zinc particles were used in the formulation of MFC/Cu films as sacrificial anode.

Figure 5 shows that zinc addition led to the formation of composite films where spherical Zn particles are homogeneously distributed among dendritic Cu particles tight together by both individual microfibrils and MFC clusters. The presence of large (5–10 μm in size) and irregular surface pores is in line with the low apparent density obtained for both MFC/Cu and MFC/Cu/Zn films Figs. 3a and 5, respectively. Figure 5 shows that a ∼150-fold increase in conductivity was obtained after Zn addition and that the abrupt conductivity increase observed after the addition of 5 % of Zn was followed by a progressive decay. This trend was interpreted as reflecting:

(i) The protective action of Cu against oxidation by Zn particles (even at low Zn mass fractions) during slurry preparation and film formation.

(ii) Owing to the insulator behaviour of zinc oxide, the progressive decrease of the volume fraction of the conducting phase (Cu) which dropped from 12 to 10 % when the Zn mass fraction was increased from 5 to 15 %.

In line with the absence of an oxide layer on copper particles, the conductivity of MFC/Cu/Zn films was not affected by a corona treatment.

The monitoring of film conductivity over time (Fig. 6) showed that, despite the good Zn protective action during the aqueous processing, natural Cu oxidation in contact with air was not suppressed and film conductivity progressively decreased by one order of magnitude in 3 day. Prolonged film ageing (2 months) led to a further decrease in conductivity and MFC/Cu/Zn films had conductivities close to that of samples without Zn (i.e. ∼11 S m^{-1}).
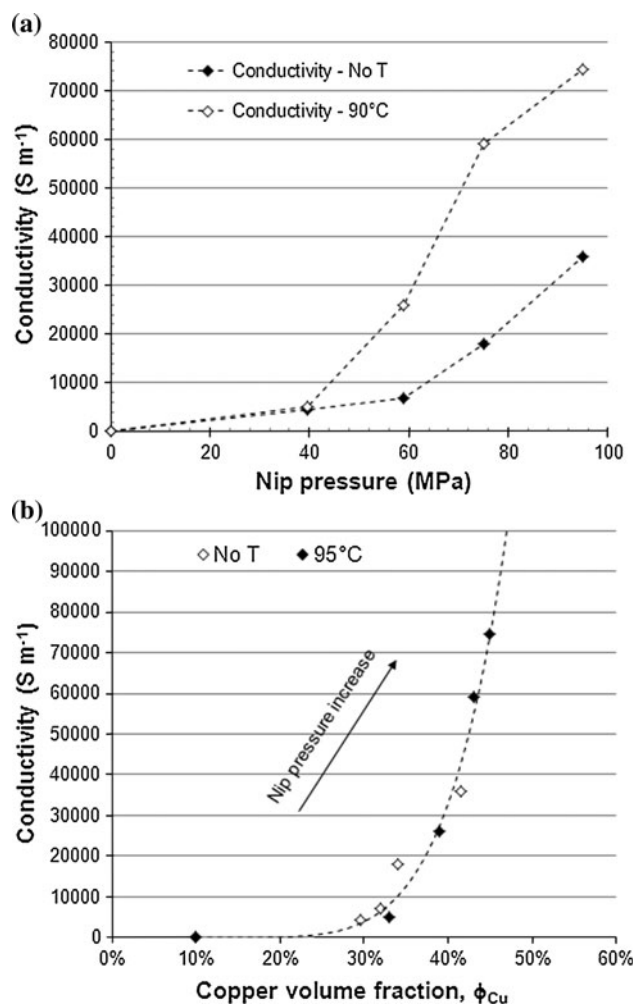

Fig. 7 Influence of: **a** the calender pressure and temperature on the conductivity of ethanol-based films with a copper weight fraction of 97 %; **b** the copper volume fraction on the conductivity of calendered films. *Dotted lines* in **b** represent data fitting with Eq. (6), $\sigma_0 = 1.9 \times 10^7$ S m^{-1}, $\phi_C = 9.5$ % and t = 5.3
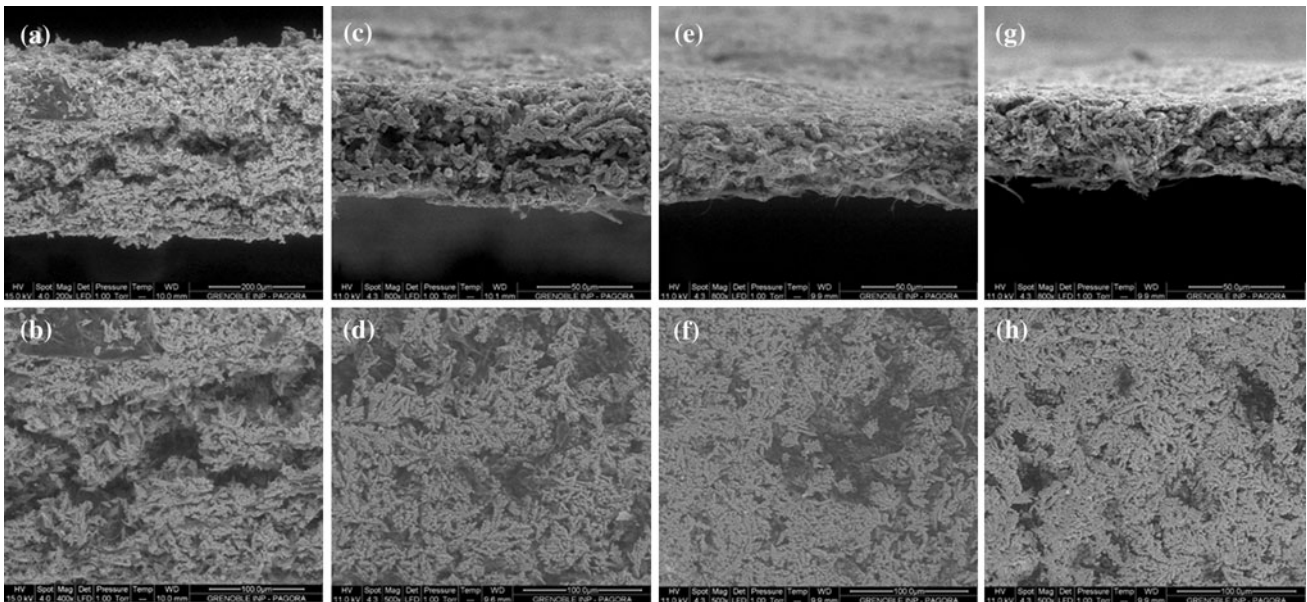
Fig. 8 SEM images of side and top views of MFC–Cu films processed in ethanol and calendered at room temperature. **a, b** No calendering, $\phi_{Cu} = 9$ %, no conductivity. **c, d** 40 MPa calendering, $\phi_{Cu} = 30$ %, $\sigma = 4.5 \times 10^3$ S m^{-1}. **e, f** 60 MPa calendering, $\phi_{Cu} = 32$ %, $\sigma = 7 \times 10^3$ S m^{-1}. **g, h** 96 MPa calendering, $\phi_{Cu} = 42$ %, $\sigma = 36 \times 10^3$ S m^{-1}
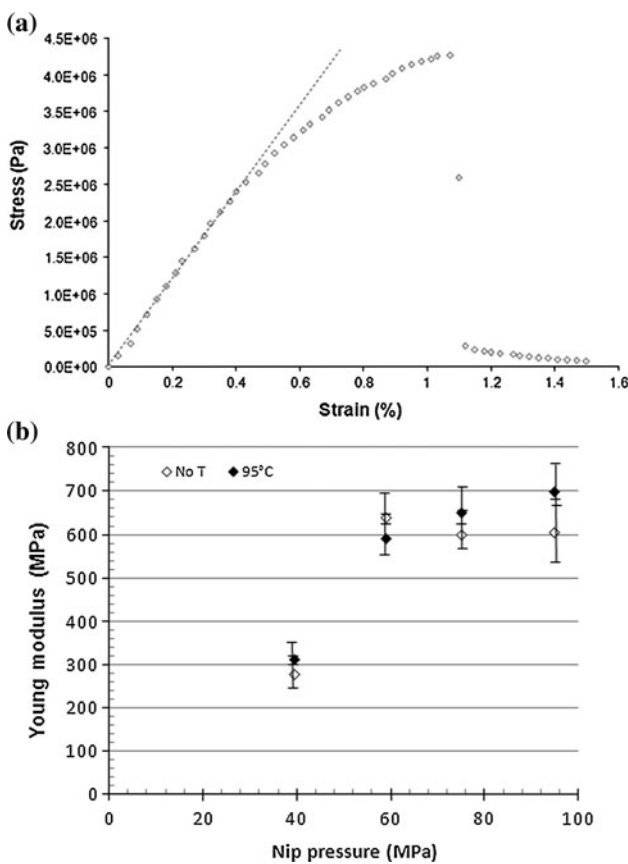

Fig. 9 Effect of film calendering on films Young's modulus. **a** Stress–strain curve of a MFC/Cu film calendered at 60 MPa and room temperature. **b** Films Young's modulus

Film densification by calendering had negligible/no impact on the conductivity of MFC/Cu and MFC/Cu/Zn films processed in water.

When ethanol was used as dispersing medium, MFC/Cu films in the presence and in the absence of Zn displayed insulator behaviour and no conductivity was detected. The absence of electron transport within the film was associated with the low film density, i.e. 915 kg m^{-3} against 1220 kg m^{-3} when using water, and with a Cu volume fraction below the percolation threshold of 9.5 %. The drop in apparent density was also reported for films made from ethanol–MFC or water–MFC mixtures [46], and associated to a lower capillary pressure in the presence of ethanol.

Figure 7a shows that, whatever the calendering temperature, samples calendering at 40 MPa led to a sharp increase in the Cu volume fraction from ca. 10 to 30 % with a conductivity increase up to 5000 S m^{-1}. The increase of the calendering pressure induced the progressive densification of MFC/Cu films and a nearly linear increase of both the Cu volume fraction and conductivity. Above 96 MPa, conductivity dropped displaying highly scattered values. Moreover, visible crackles appeared on MFC/Cu films indicating the onset of film damage and the disconnection of conductive paths.

Films calendered at 90 °C had better conductivity than those processed at room temperature. Since 90 °C is a temperature too low to promote copper sintering, higher conductivity was associated to an increase in copper malleability and, as supported by a 5–10 % increase in the Cu

Fig. 10 Variation of the thickness of MFC/Cu films screen printed on copy paper as a function of the number of passes. *Inset* shows images and SEM pictures of MFC/Cu films
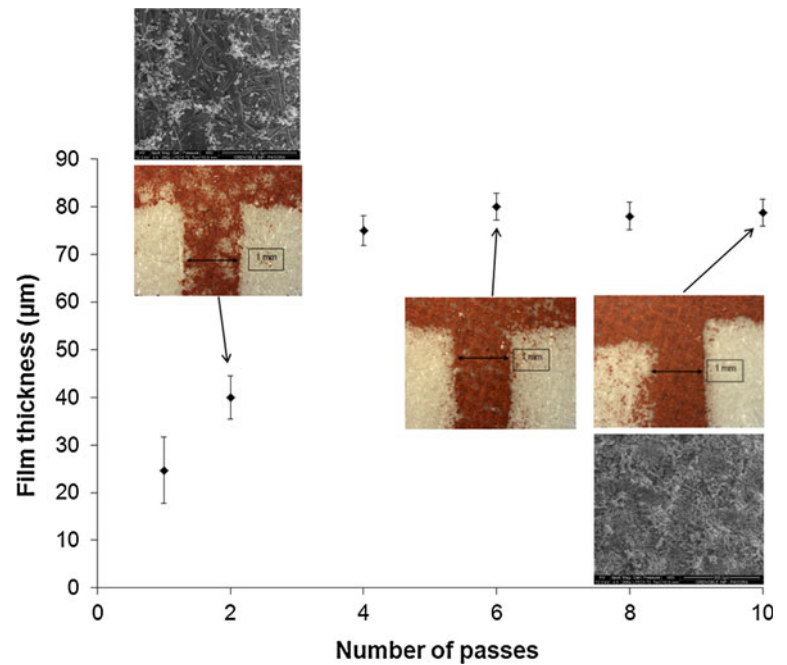

Table 1 Conductivity and resistance values of MFC/Cu films obtained by Mayer rod coating and screen printing on copy paper (10 passes)

Deposition technique	Film property	Bare film	Film + corona	Film + calendering	Film + calendering + corona
Coating	Resistance (Ω sq^{-1})	∞	6.8×10^7	3200	140
	Thickness (μm)	150	150	75	75
	Conductivity (S m^{-1})	No conductivity	3×10^{-4}	4.2	95
Screen Printing	Resistance (Ω sq^{-1})	∞	1.8×10^4	10^8	70
	Thickness (μm)	75	75	25	25
	Conductivity (S m^{-1})	No conductivity	0.7	4×10^{-4}	570

volume fraction, to a denser particle packing at high temperature. The dominant effect of a more pronounced material densification at higher temperature is supported by the plot of film conductivity versus the copper volume fraction shown in Fig. 7b. Indeed, data obtained for films calendered at room temperature and 90 °C lie on a master curve that can be interpolated with the typical equation describing electron transport in conductive composites [47]

$$\sigma = \sigma_0 (\phi - \phi_C)^t. \tag{6}$$

where σ_0 is the conductivity of the conductive filler, ϕ is its volume fraction and ϕ_C the percolation threshold. The percolation threshold obtained by the interpolation with Eq. (6) of experimental data, i.e. 9.5 %, was in line with the ϕ_C value determined for Cu particles processed in water (Fig. 3) thus, confirming that different particle packing and Cu surface oxidation were the two dominating factors affecting the conductivity of MFC/Cu film cast from water and ethanol suspensions.

Pictures shown in Fig. 8 illustrate the effect of calendering on the progressive film densification and the formation of closely packed surface and bulky conductive pathways.

The addition of zinc to MFC/Cu slurries in ethanol had no impact on film conductivity, thus indicating that copper oxidation can be effectively prevented using an ethanol-based slurry formulation.

Stress–strain tests showed that all MFC/Cu films displayed the same general brittle behaviour illustrated in Fig. 9a with a first elastic behaviour followed by a plastic transition and the break at a strain of ca. 1 %. Figure 9b shows that the Young's modulus of calendered films varied between 300 and 700 MPa with values far below copper (124 GPa), MFC films (10 GPa [31]) and single cellulose microfibril (140 GPa [33]). The low Young's modulus of MFC/Cu composites was associated to the high film porosity and the presence of "unbound" copper particles. Below a nip pressure of 60 MPa, the increase of the Young's modulus was ascribed to film densification, a drop

in film thickness (Fig. 8), of its cross sectional area and a subsequent increase of the applied stress. Whereas, above 60 MPa, film thickness remains nearly constant and the Young's modulus attains a plateau.

The increase of the calendering temperature seems to positively affect the film modulus. However, owing to highly scattered experimental values, the contribution of temperature could not be clearly assessed.

In order to evaluate the processability of MFC/Cu aqueous slurries, conductive coatings were deposed on copy paper by Mayer rod coating and screen printing using MFC/Cu slurries with a dry solid content of 22 % (97 % Cu and 3 % MFC).

Homogeneous and up to 150 μm thickness films were easily obtained by rod coating, whereas several passes were needed when using screen printing (Fig. 10). The thickness of screen printed films increased with the number of passes attaining a maximum of about 75 μm after 4 passes, when, as shown in Fig. 10, a homogeneous film was formed. The further increase of the number of passes had no effect on film thickness indicating that MFC/Cu slurry transfer on the substrate was limited by the screen design used in this study.

Owing to the absence of Zn particles and to their low bulk density, MFC/Cu films deposed on copy papers had a resistive behaviour. Films treatment by corona discharge (20 s) or calendering (90 MPa) conferred to the films a slight conductive behaviour. Whereas, film treatment by both calendering and corona discharge led to high conductivity values (Table 1) thus, showing that MFC/Cu aqueous slurries can be used for the elaboration of conductive coatings on paper substrates. The addition of Zn in the aqueous slurry led to a further increase in the film conductivity.

Conclusion

This study demonstrated that highly conductive films can be elaborated using copper particles and MFC as binder. The high bonding ability of MFC allowed obtaining self-standing MFC/Cu films even in the presence of an extremely low MFC weight fraction. The increase of the copper weight fraction led to an increase of film conductivity up to 97 %. Above this value the formed films were no longer self-standing.

The typical oxidation of copper in the presence of water limited the conductivity of MFC/Cu films below 11.5 S m^{-1}. Copper etching with a prolonged corona discharge slightly increased film conductivity to 75 S m^{-1}, whereas, a sound increase in conductivity (up to 2500 S m^{-1}) was obtained using zinc particles as sacrificial anode in the MFC/Cu slurry formulation.

The substitution of water with ethanol as dispersing medium limited copper oxidation but induced a drop in film conductivity, which was ascribed to the low density of MFC/Cu films processed in ethanol, i.e. 915 kg m^{-3} against 1220 kg m^{-3} of films processed in water.

Ethanol-based films densification by calendering improved film conductivity and Young's modulus up to 70000 S m^{-1} and 600 MPa, respectively.

The use of MFC/Cu slurries for the elaboration of conductive coatings was assessed using Mayer rod coating and screen printing. In both cases corona treatment and film calendering were necessary to obtain conductive films, however similar and even higher conductivities can be obtained using Zn particles as sacrificial anode in aqueous formulations or ethanol-based MFC/Cu slurries.

References

1. Forrest SR (2004) Nature 428:911
2. Nishide H, Oyaizu K (2008) Science 319:737
3. Li Y, Rida M, Vyas R, Tentzeris MM (2007) Microwave Theory Tech, IEEE Trans 55:2894
4. Abad E, Zampolli S, Marco S, Scorzoni A, Mazzolai B, Juarros A, Gomez D, Elmi I, Cardinali GC, Gomez JM, Palacio F, Cicioni M, Mondini A, Becker T, Sayhan I (2007) Sens Actuators B 127:2–7
5. Chung I-J, Kang I (2009) Mol Cryst Liq Cryst 507:1
6. Hilder M, Winther-Jensen B, Clark NB (2009) J Pow Sour 194:1135
7. Perelaer J, Smith PJ, Mager D, Soltman D, Volkman SK, Subramanian V, Korvink JG, Schubert US (2010) J Mater Chem 20:8446
8. Ng SH, Wang J, Guo ZP, Chen J, Wang GX, Liu HK (2005) Electrochim Acta 51:23
9. Chen J, Liu Y, Minett AI, Lynam C, Wang J, Wallace GG (2007) Chem Mater 19:3595
10. Kaempgen M, Chan CK, Ma J, Cui Y, Gruner G (2009) Nano Lett 9:1872
11. Pushparaj VL, Shaijumon MM, Kumar A, Murugesan S, Ci L, Vajtai R, Linhardt R, Nalamasu O, Ajayan P (2007) PNAS 104:13574
12. Hu L, Choi JW, Yang Y, Jeong S, La Mantia F, Cui L-F, Cui Y (2009) PNAS 106:21490
13. Frackowiak E, Gautier S, Gaucher H, Bonnamy S, Beguin F (1999) Carbon 37:61
14. Chen H, Müller MB, Gilmore KJ, Wallace GG, Li D (2008) Adv Mater 20:3557
15. Chung DDL (2002) J Mater Sci 37. doi:10.1023/A:1014915307738
16. Liu Y, Treadwell DR, Kannisto MR, Mueller BL, Laine RM (1997) J Am Ceram Soc 80:705
17. Park BK, Kim D, Jeong S, Moon J, Kim JS (2007) Thin Solid Films 515:7706
18. Lee B, Kim Y, Yang S, Jeong I, Moon J (2009) Curr Appl Phys 9:157
19. Dearden AL, Smith PJ, Shin D-Y, Reis N, Derby B, O'Brien P (2005) Macromol Rapid Commun 26:315

20. Kamyshny A, Ben-Moshe M, Aviezer S, Magdassi S (2005) Macromol Rapid Commun 26:281
21. Nur HM, Song JH, Evans JRG, Edirisinghe MJ (2002) J Mater Sci 13. doi:10.1023/A:1014827900606
22. Kang JS, Kim HS, Ryu J,Hahn HT, Jang S, Joung JW (2010) J Mater Sci 21. doi:10.1007/s10854-009-0049-3
23. Mori k, Okai Y, Yamada H, Kashiwaba Y (1993) J Mater Sci 28. doi:10.1007/BF00357810
24. Ota T, Fukushima M, Ishigure Y, Unuma H, Talahashi M, Hikichi Y (1997) J Mater Sci Lett 16. doi:10.1007/BF02765404
25. Xue Q (2004) Eur Polym J 40:323
26. Luyt AS, Molefi JA, Krump H (2006) Polym Degrad Stab 91:1629
27. Tekce HS, Kumlutas D, Tavman IH (2007) Reinf Plast Compos 26:113
28. Pavlovic MM, Cosovic V, Pavlovic MG, Talijan N, Bojanic V (2011) Int J Electrochem Sci 6:3812
29. Herrick FW, Casebier RL, Hamilton JK, Sandberg KR (1983) J Appl Polym Sci Appl Polym Symp 37:797
30. Turbak AF, Snyder FW, Sandberg KR (1983) J Appl Polym Sci: Appl Polym Symp 37:815
31. Siró I, Plackett D (2010) Cellulose 17:459
32. Lu J, Wang T, Drzal LT (2008) Composites A 39:738
33. Iwamoto S, Kai W, Isogai A, Iwata T (2009) Biomacromolecules 10:2571
34. Janardhnan S, Sain M (2006) Bioresources 1:176
35. Sain M, Oksman k (2006) ACS Symp Ser Cellul Nanocompos 938:2
36. Sasso C, Zeno E, Petit-Conil M, Chaussy D, Belgacem MN, Tapin-Lingua S, Beneventi D (2010) Macromol Mater Eng 295:934
37. Jabbour L, Gerbaldi C, Chaussy D, Zeno E, Bodoardo S, Beneventi D (2010) J Mater Chem 20:7344
38. Sehaqui H, Liu A, Zhou Q, Berglund LA (2010) Biomacromolecules 11:2195
39. Liu A, Walther A, Ikkala O, Belova L, Berglung LA (2011) Biomacromolecules 12:633
40. Leijonmarck S, Cornell A, Lindbergh G, Wågberg L (2013) Nano Energy in press
41. Leijonmarck S, Cornell A, Lindbergh G, Wågberg L (2013) J Mater Chem 1:4671
42. Guérin D, Chaussy D (2009) Techniques de l'ingénieur. BM 7(411):1
43. Lux F (1993) J Mater Sci 28. doi:10.1007/BF00357799
44. Sun QC, Zhang DD, Wadsworth LC (1998) Tappi J 81:177
45. Milazzo G, Caroli S (1978) Tables of Standard Electrode Potentials. Wiley, New York, p 437
46. Henriksson M, Berglund LA, Isaksson P, Lindström T, Nishino T (2008) Biomacromolecules 9:1579
47. Kirkpatrick S (1973) Rev Mod Phys 45:574